Cytoskeletal mechanics of neurulation: insights obtained from computer simulations

G. Wayne Brodland and David A. Clausi

Abstract: The morphogenetic movements associated with the process of neurulation have been the subject of much investigation during the last one hundred years. A plethora of experimental evidence has been generated regarding the forces that drive this seemingly simple process, and many theories about the mechanics of the process have been proposed. Recent computer simulations have proved useful for evaluating these theories from a mechanical perspective. In this work, computer simulations are used to investigate several theories about the forces that drive neurulation. A simplified version of a formulation previously presented by the authors provides the mathematical foundation for these simulations. The simulations confirm that forces generated by circumferential microfilament bundles (CMB's) in conjunction with notochord forces can produce the rolling motions characteristic of amphibian neurulation. They also support the notion that redundancies exist in the systems of forces available to drive neurulation shape changes. The shape changes that occur following a variety of surgical and teratogenic interventions are also simulated. These simulations corroborate the role of circumferential microfilament bundles as a primary force generator.

Key words: neurulation, cytomechanics, computer simulations, finite element method.

Résumé : Les mouvements morphogénétiques associés au processus de la neurulation ont fait l'objet de plusieurs études au cours du dernier siècle. Une multitude de résultats expérimentaux concernant les forces entraînant ce processus apparemment simple ont été obtenus et plusieurs théories sur la mécanique de ce processus ont été proposées. De récentes simulations par ordinateur se sont montrées utiles pour évaluer ces théories au point de vue mécanique. Dans ce travail, des simulations par ordinateur ont été utilisées pour évaluer plusieurs théories sur les forces entraînant la neurulation. Ces simulations sont basées sur une version simplifiée d'une expression mathématique publiée antérieurement par les auteurs. Elles confirment que les forces générées par les faisceaux de microfilaments apicaux associées aux forces de la chorde dorsale peuvent produire les mouvements d'enroulement caractéristiques de la neurulation chez les amphibiens. Ces simulations appuient également la notion qu'il y a redondance des systèmes de forces disponibles pour entraîner les changements de forme durant la neurulation. Les changements de forme se produisant à la suite de diverses interventions chirurgicales et tératogènes ont également été simulés. Ces simulations corroborent le rôle des faisceaux de microfilaments apicaux en tant que générateurs principaux de la force.

Mots clés : neurulation, cytomécanique, simulations par ordinateur, méthode des éléments finis.

[Traduit par la rédaction.]

Introduction

The seemingly simple process of neurulation has been the subject of intensive investigation for more that one hundred years (Roux 1888; Gordon 1985; Koehl 1990; Schoenwolf and Smith 1990; Clausi and Brodland 1993). In most vertebrates, the morphogenetic movements that accompany neurulation include motions in the plane of the neural plate and rolling of the plate into a closed tube. Neurulation is an important process because irregularities in it can give rise to a variety of common human birth defects (Campbell et al. 1986; Copp et al. 1990).

Received January 23, 1995. Accepted May 9, 1995.

Abbreviations: CMB, circumferential microfilament bundles.

G.W. Brodland and D.A. Clausi. Departments of Civil Engineering and Systems Design Engineering, University of Waterloo, Waterloo, ON N2L 3G1, Canada.

Much attention has been devoted to identifying the sources of the mechanical forces that drive the morphogenetic movements critical to neurulation (His 1874; Burt 1943; Lewis 1947; Balacinsky 1961; Jacobson 1978; Lee and Nagele 1988; Smith and Schoenwolf 1991). The shape changes which the neural plate undergoes are now well known (Burnside and Jacobson 1968; Jacobson and Löfberg 1969), as are the morphology (Fig. 1) and mechanical nature of its cytoskeleton and other force producing structures (Burnside 1973; Rappaport 1977; Hill and Kirshner 1982*a*, 1982*b*; Brodland and Gordon 1990). Numerous surgical and teratogenic experiments have also been carried out in an effort to elucidate the mechanics of neurulation (Jacobson and Gordon 1976; Copp et al. 1990; Schoenwolf and Smith 1990).

Experimental studies by themselves, however, have failed to settle such fundamental issues as the importance to neural tube morphogenesis of microfilaments, the notochord, and various other possible extrinsic forces (Clausi and Brodland

Fig. 1. Cytoskeletal components and other subcellular features that may be of mechanical importance to neural plate morphogenesis (after Clausi and Brodland 1993).

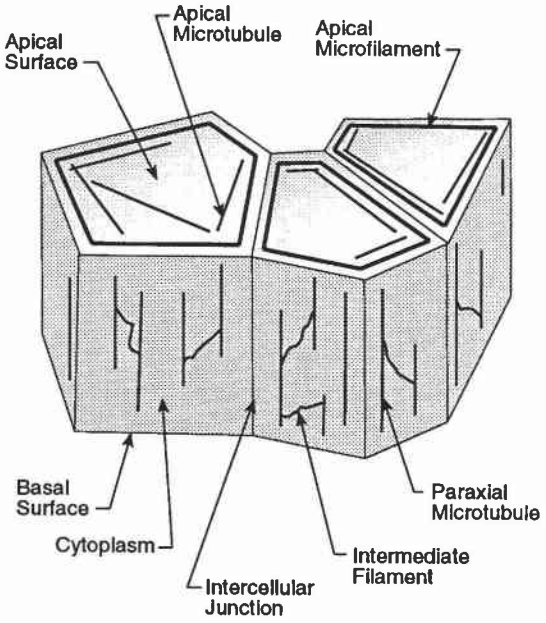

1993). As intriguing aspects of neural tube closure, such as cell skewing at the junction between the neural plate and neural ridge (Jacobson et al. 1986) and the appearance of hinges during neural tube closure (Smith and Schoenwolf 1991), receive attention, novel theories continue to arise. Difficulties in resolving mechanical issues about neurulation arise because the shape changes that occur are three dimensional, mechanical interactions apparently occur between the plate and adjacent tissues, and multiple force systems may contribute to the shape changes observed (Clausi and Brodland 1993).

Computer simulations have come to be accepted as a complement to experimental studies and intuitive arguments (Jacobson and Gordon 1976; Jacobson 1980; Odell et al. 1981; Hilfer and Hilfer 1983; Jacobson et al. 1986; Weliky and Oster 1990, Clausi and Brodland 1993; Brodland 1994; Brodland and Clausi 1994). They can be used to investigate both kinematic and kinetic aspects of morphogenetic movements. If they are suitably formulated, they can also be used to determine the shape changes that specific sets of driving forces would produce, and thus serve to test hypotheses about the forces that drive particular morphogenetic movements. Advantages that such simulations have over experimental studies are that adjustments of arbitrary size can be made with accuracy in any chosen parameter, and that these can be made without concern that other properties might be affected at the same time.

The purpose of this work is to use computer simulations similar to those developed by Brodland and Clausi (1994) to further investigate hypotheses regarding the forces that drive neurulation. For the class of problems considered here, a somewhat simplified formulation can be used. To test each hypothesis, the system of driving forces set forth in the hypothesis is applied to a flat plate of tissue (actually, a transverse strip from such a plate). The computer simulation determines the sequence of shape changes that each system of forces would produce in the initially flat strip. Specific shapes from these sequences can then be compared with transverse cross-sections that occur in live embryos. Since the patterns of shape change produced in the simulations are highly sensitive to details of the applied forces, meaningful comparisons can be made. A variety of experiments that involve surgical intervention or use of teratogens are also simulated. Jointly, the simulations uphold the view that apical microfilament contraction and notochord elongation provide the primary driving forces during neurulation. They also support the concepts of cooperation of forces and regional differences (Brun and Garson 1983; Schoenwolf and Smith 1990).

Forces generators

Figure 1 illustrates subcellular components typically found in epithelial cell sheets. The components considered in this work include microfilaments, microtubules, intermediate filament networks, cell cytoplasm, and cell membranes. The mechanical properties of these components relevant to neurulation have been reviewed in Brodland and Clausi (1994) and only their main features are reiterated here.

Microfilaments occur in circumferential microfilament bundles (CMBs) at the apical end of neural plate cells. They are contractile and intercalate as the bundle shortens so that the cross-sectional area of the bundle increases during shortening in such a way as to maintain the volume of the microfilament bundle (Burnside 1971; Rappaport 1977; Alberts et al. 1989).

Microtubules, in contrast, are assumed to exert forces as a result of axial polymerization (Hill 1981; Hill and Kirshner 1982*a*, 1982*b*). Like Hart and Trainor (1990), we model the mechanical effects of apical microtubules and microfilaments together.

To measure the bulk mechanical properties of cytoplasm, various methods have been used (Hiramoto 1969; Valberg and Alvertini 1985). These tests use strain rates that are magnitudes higher than those that occur during morphogenetic movements. As a consequence, known estimates of cytoplasmic properties probably involve tearing of the intermediate filament meshwork that courses through the cells (Brodland and Gordon 1990) and do not provide numerical values that are applicable to the low strain rates typical of morphogenesis. Like Brodland and Gordon (1990), we represent the cytoplasm, including any intermediate filament mesh that might be present, as a single isotropic material.

Membrane forces caused by intercellular adhesions and by cell membrane tension (Alberts et al. 1989) are, under the circumstances of interest here, nearly equivalent to those produced by microfilaments and microtubules (Brodland and Clausi 1994). Here, we group all of these together into an equivalent microfilament force. This approach modifies the line of action of some forces and does not fully accommodate the distinctive ways in which forces produced by specific cytoskeletal components change with deformation. However, this approach is generally consistent with the degree of detail accommodated by the present model. It also significantly reduces the number of parameters that must be investigated and prevents the principal mechanical arguments from becoming obscured by minor ones.

Formulation

A finite element-based formulation similar to that developed by Brodland and Clausi (1994) is presented here. The new formulation is somewhat simplified and more intuitive. It will model viscous materials accurately, but unlike the original formulation, cannot, in general, model the broader class of viscoelastic materials. This is not a serious limitation since the previous study suggested that, during neurulation, viscous behaviour governs the shape changes that occur. The present formulation also satisfies the technical criteria for computer simulations of morphogenetic processes outlined by Gordon (1985) and Brodland and Clausi (1994).

Representation of active cytoskeletal components

Cytoskeletal components such as microfilaments and microtubules act as motors that drive morphogenetic movements. In this sense they are active. Because of their specific morphologies, they and other mechanically equivalent force generators like cell membranes, can be modelled as bar or truss elements along the borders of cells in simulations of neurulation (Brodland and Clausi 1994). Two versions of truss elements are used in the simulations.

In one version, the truss force f is assumed to depend on the inverse of its length. This force–length relationship is ideal for modelling a microfilament bundle because although the stress (force/area), $\boldsymbol{\sigma}$, it produces remains constant, the cross-sectional area of such a bundle at any instant depends on its initial cross-sectional area A_0 and the ratio of its initial length L_0 to its current length L. The force in these elements is, therefore, assumed to follow the relationship

$$[1] \quad f = \boldsymbol{\sigma} \cdot A_0 \cdot \frac{L_0}{L}$$

In the other version of these elements, the truss force is assumed to remain constant. These elements can also be used to model microtubules, or microfilaments whose force is assumed to remain constant. The force f is written in terms of a stress, $\boldsymbol{\sigma}$, and an initial area, A_0, using the formula

$$[2] \quad f = \boldsymbol{\sigma} \cdot A_0$$

The syntax of equation 2 is chosen to permit direct comparison with equation 1. When a mix of microfilaments, microtubules, and other active components are present, that ensemble would generate a force that is both between the forces given by the idealized relationships of equations 1 and 2, and dependent on the nature and degree by which the ensemble force is affected by deformation.

Representation of cell volumes

Eight-noded viscous isoparametric volume elements are used to represent volumetric components such as cell cytoplasm. In standard finite element formulations, a stiffness matrix is derived for each element in the structure. It relates the forces at each of the corners or nodes of an element to the elastic displacements that occur at each corner. The elemental stiffness matrix, K_e^i, for an eight-noded isoparametric volume element filled with an isotropic, elastic material is available in standard finite element texts (Huebner and Thornton 1982; Logan 1986; Zienkiewicz and Taylor 1989). For studies of neurulation, an elemental matrix is required for this geometry but for an isotropic viscous material. The Alfrey–Henry analogy can be used to transform the elemental stiffness matrix into an elemental viscosity matrix, $\overline{K}_e^i$, relating nodal forces to nodal rates of displacement. The resulting viscosity matrix is

$$[3] \quad \overline{K}_e^i = \int_V B^T C B \, dV$$

where the matrix B relates element nodal rates of displacement to element strain rates, $\dot{\varepsilon}$, according to

$$[4] \quad \dot{\varepsilon} = B \cdot \dot{u}$$

and C relates element strain rates to element stresses according to the constitutive equation

$$[5] \quad \boldsymbol{\sigma} = C \cdot \dot{\varepsilon}$$

The integration is performed over the volume, V, of the element. For a three-dimensional isotropic viscous material, the matrix C in equation 5 may be written as

$$[6] \quad C = \mu \begin{bmatrix} \frac{2(1-\nu)}{1-2\nu} & \frac{2\nu}{1-2\nu} & \frac{2\nu}{1-2\nu} & 0 & 0 & 0 \\ \frac{2\nu}{1-2\nu} & \frac{2(1-\nu)}{1-2\nu} & \frac{2\nu}{1-2\nu} & 0 & 0 & 0 \\ \frac{2\nu}{1-2\nu} & \frac{2\nu}{1-2\nu} & \frac{2(1-\nu)}{1-2\nu} & 0 & 0 & 0 \\ 0 & 0 & 0 & \frac{1-2\nu}{2} & 0 & 0 \\ 0 & 0 & 0 & 0 & \frac{1-2\nu}{2} & 0 \\ 0 & 0 & 0 & 0 & 0 & \frac{1-2\nu}{2} \end{bmatrix}$$

where μ and ν are the bulk shear viscosity and Poisson's ratio, respectively, for the element material.

Experiments have shown that, in amphibians, cell volume is maintained during neurulation even when mitoses occur (Burnside and Jacobson 1968). When ν approaches 0.5 (e.g., $\nu = 0.49$), so that volume is maintained, full Gauss quadrature can not be used, because it gives rise to numerical difficulties (note the denominators of many of the terms in equation 6) and element locking (Belytschko and Ong 1984). Reduction of the integration order to eliminate locking results in spurious zero-energy modes of deformation called hourglass modes. In the simulations presented here, reduced order integration is used and hourglassing is controlled using a technique devised by Liu et al. (1985).

Solution procedure

When a specific force, such as that produced by a certain microfilament bundle, acts on a cell or group of cells, the specific deformation that will be produced can be calculated using equations 1–6. However, as the cells deform, the structure on which the force generator acts changes. It is then nec-

essary to consider a new problem, namely one in which the microfilament bundle acts on a new geometry. In addition, if the microfilament force is given by equation 1, the applied force may have to be updated because L has changed. In the formulation used here, the neurulation process is broken into a succession of short intervals. For each time step, the incremental displacement produced during that time step is calculated. At the end of each time step, the geometry of the structure is updated and applied forces are recalculated in preparation for the next time step. This approach is the basis of an updated explicit Lagrangian scheme (Zienkiewicz and Taylor 1991) like that used here.

During the i^{th} time step, the behaviour of the epithelium as a whole will be given by the equation

$$[7] \quad f^i = \overline{K}^i \cdot \dot{u}^i$$

where f^i is a vector of unbalanced nodal forces acting at the beginning of the i^{th} time step, formed by assembly of elemental forces (Logan 1986; Zienkiewicz and Taylor 1989), and $\overline{K}^i$ is the global viscosity matrix of the system (analogous to a stiffness matrix) at the beginning of the i^{th} time step, formed by assembly of the elemental stiffness matrices $\overline{K}_e^i$, and $\dot{u}^i$ is the vector of rates of nodal displacement (nodal velocities) during the i^{th} time step.

The total displacement, u^i, at the end of the i^{th} time step is

$$[8] \quad u^i = u^{i-1} + \Delta t^i \cdot \dot{u}^i$$

where u^0 is the vector of initial nodal positions and Δt^i is the length of the i^{th} time step. Time steps are chosen sufficiently small that solution divergence does not occur and that numerical errors do not accumulate. Optimal step size depends on the extent of the nonlinearities acting at any particular step and, therefore, may vary from step to step. All geometries and forces are updated with each time step.

A variety of checks are performed to ensure solution accuracy. These include verifications that the element volumes do not change, and tests to ensure that the step sizes used are small enough that the solution is not step-size dependent.

Simulations of hypothesized neural-plate conditions

The simulations reported in this section are designed to investigate features of neural plate reshaping that would be apparent in transverse sections. For this purpose, a transverse strip from the left side of an embryo is modelled (Fig. 2A). The strip has a width, w, of 120 μm in the cephalo–caudal direction and has an initial height h, or thickness of 120 μm. An assemblage of 20 finite elements, each 40 (medio–lateral dimension) × 120 (cephalo–caudal dimension) × 120 μm tall is used to model the part of the strip taken from the neural plate. Twenty geometrically identical elements model the attached nonneural ectoderm. Each of these finite elements can be thought of as modelling one cell, 40 × 120 × 120 μm tall, or three cells, each 40 × 40 × 120 μm tall. Alternatively, the elements might be thought of as representing discrete parts of a sheet of randomly shaped cells. In the latter interpretation, the finite element boundaries do not correspond to cell boundaries. This does not pose a problem provided that the elements are assigned the bulk mechanical properties of the sheet (Brodland and Clausi 1994). The authors prefer the latter interpretation because it accommodates more naturally the continuous cell–cell neighbour changes that occur typically during plate morphogenesis.

Fig. 2. Reference case. (A) A strip of tissue from the left side of a transverse section of a neural plate. The strip is 120 μm tall, and its dimension in the cephalo–caudal direction is 120 μm. The strip is modelled by 40 volume finite elements, with truss elements on the apical surface of the neural plate (indicated by wider lines) representing CMBs. Microfilament contraction is modelled using equation 1. The cephalo–caudal dimension of the strip doubles by $\tau = 17$ and the medial edge of the plate is allowed to move towards the mid-sagittal plane at a constant rate of 56 μm·θ. This simulation is known as the reference case. Parts B through F of the figure illustrate the sequence of shape changes produced by the joint action of microfilament forces and cephalo–caudal elongation. See text for further details.

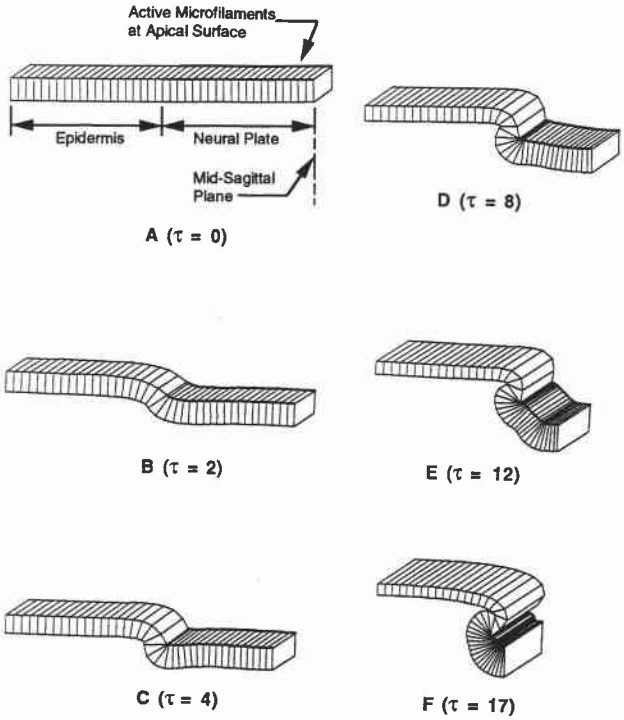

Reference case

In the first simulation, microfilaments (truss elements) are added along the apical surface of those elements that represent neural plate cells. The positions of the microfilaments are indicated by wider lines in Fig. 2. For these simulations, the microfilament forces increase as the microfilament shortens, in accordance with equation 1, and their magnitude is given by

$$[9] \quad F_A = \frac{N_{MF}\sigma A_0}{\mu w h \theta} = 0.10$$

where N_{MF} is the number of microfilament bundles across the width of the strip, μ is the viscosity of the cytoplasm, and θ is a dimensionless time parameter.

The dimensionless force given by equation 9 serves to provide similitude between a broad family of simulations, including some with differing time scales. To illustrate the effect of time scaling, consider the effect of doubling only the viscosity of the cytoplasm. Identical sequences of shape change would be produced, except that twice as much time would be

required to reach any specified degree of deformation. By including a time scaling factor, θ, with units of time^{-1}, such simulations can also be mapped into one. Simulations are then reported in terms of a dimensionless time,

[10] $\tau = t \cdot \theta$

where t is actual time.

During normal neural plate morphogenesis, the plate elongates and its edges move medially. On the basis of time lapse images of axolotl neurulation collected in our laboratory, these effects are modelled by moving the lateral edge of the nonneural ectoderm medially at a rate of 56 μm·θ and by axially elongating the strip so that its cephalo–caudal dimension doubles by $\tau = 17$.

Figure 2 shows the shape changes that would occur in a mechanical system with the geometry, boundary conditions, and mechanical properties just described. This system is here referred to as the reference case. By $\tau = 2$ (Fig. 2B), a distinct neural ridge is apparent and cell skewing (Jacobson et al. 1986; Brodland and Shu 1992) is visible at the junction between the neural plate and the non-neural epithelium. By $\tau = 4$ (Fig. 2C), the neural ridge, a boundary layer phenomenon (Clausi and Brodland 1993), becomes sharply defined. The most apparent further change by $\tau = 8$ (Fig. 2D) is substantial narrowing and thickening of the neural plate while it remains relatively flat. A hinge then forms (Fig. 2E) and the plate completes the process of forming a tube (Fig. 2F).

This simulation demonstrates that in the presence of axial elongation, the salient features of neural tube formation — ridge formation, plate narrowing and thickening, cell skewing, formation and angulation at hinge points, and closure and rounding — can all be produced in the proper sequence by the action of apical constriction (CMB) forces. The simulation is based entirely on established properties of the neural plate cells and the properties of their cytoskeletal components. No use is made of cell programs, cortical tractoring (Jacobson et al. 1986), or biochemical controls or signals. This simulation raises a number of questions that we now attempt to answer.

No axial elongation

Is the pattern of shape changes altered if there is no elongation in the axial direction? Figure 3 shows a simulation that is identical to the reference case except that no axial elongation occurs. Both the neuroepithelium and nonneural ectoderm are thicker than in the reference case. When axial elongation occurs, each area of the plate and nonneural ectoderm must thin or narrow so as to maintain constancy of volume (Burnside and Jacobson 1968). In the absence of axial elongation, this component of thinning and narrowing is not present, the neural ridge is higher, and the tube rolls up somewhat more quickly.

Constant apical force

What happens if the apical (microfilament) force remains constant as described by equation 2 rather than increasing with element shortening according to equation 1? The result of such a simulation is shown in Fig. 4. Here, in contrast to the reference case, a hinge does not form at the midline, the plate does not remain flat, and even over the extended period of this simulation, does not form a closed tube.

Fig. 3. No axial elongation. This simulation is identical to the reference case, except that the boundary conditions on the cephalo–caudal borders of the strip prevent axial elongation. Compared with the reference case, both the neural plate and the nonneural ectoderm remain thicker and the tube forms more quickly. (A) Starting configuration. (B–F) Illustrations of the sequence of shape changes produced.

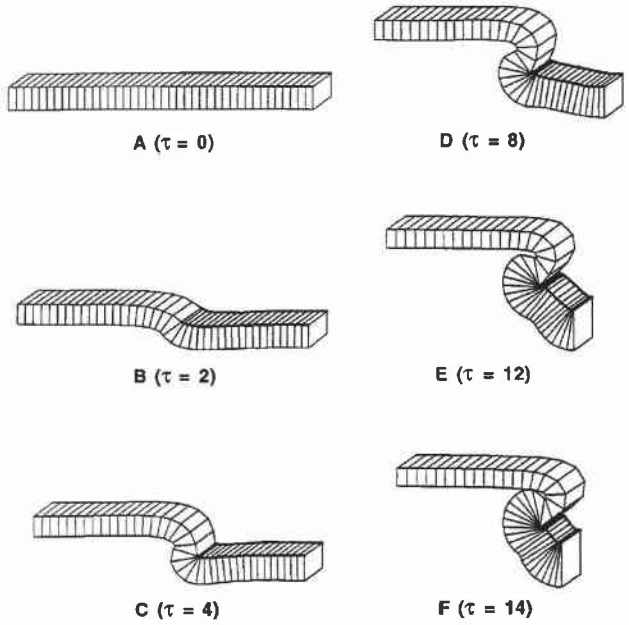

Fig. 4. Constant apical force. In this simulation, the microfilament force is modelled by equation 2 rather than equation 1. The neural plate does not remain flat, distinct hinges do not form, and the tube does not close. (A) Starting configuration. (B–D) Illustrations of selected sequence shapes produced.

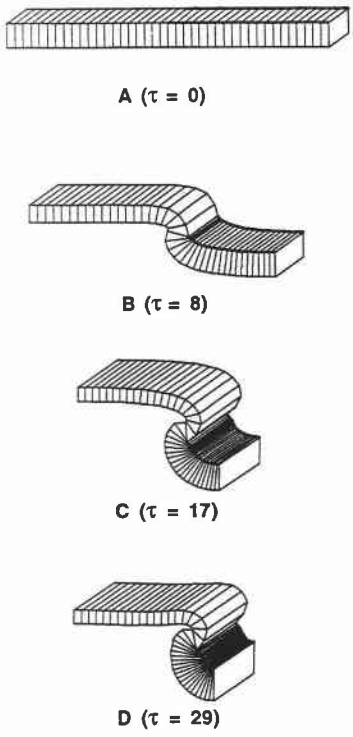

Fig. 5. Thinner plate. When the epithelium is thinner than that in the reference case, additional hinges form and plate rolling is accelerated. (A) Starting configuration. (B–E) Illustrations of selected sequential shapes produced.

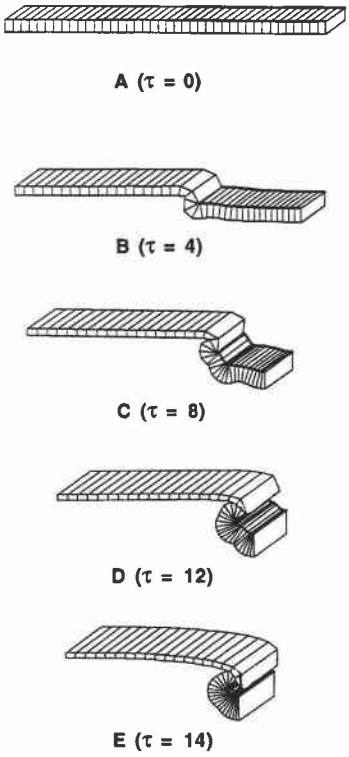

Fig. 6. Extrinsic pushing forces. When medially directed extrinsic forces act at the medial edge of the neural plate, a distinct neural ridge is not produced and no hinges form. (A) Starting configuration. (B–D) Illustrations of selected sequential shapes produced by extrinsic forces.

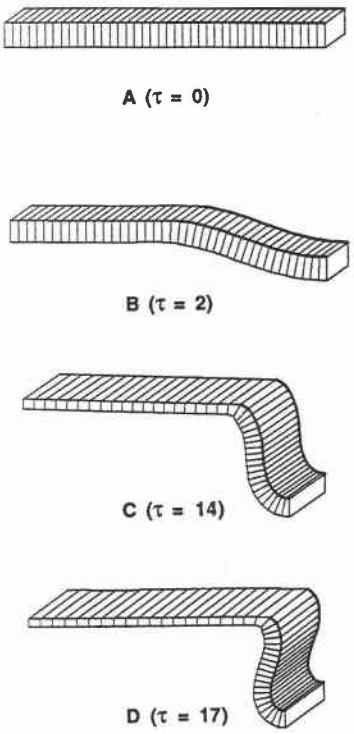

Thinner epithelium

How important is the thickness of the epithelium? Figure 5 shows a simulation in which the plate begins half as thick as that in the reference case. A sharper and narrower neural ridge is formed, the midline hinge forms earlier, and an additional hinge develops.

Extrinsic forces

Is it possible that transverse features of neural plate reshaping are caused by forces extrinsic to the neural plate? Several lines of argument have provided support for this concept (Schoenwolf and Smith 1990). The simulation shown in Fig. 6 answers this question. A medial force of magnitude

$$[11] \quad F_M = \frac{F_{\text{Medial}}}{\mu w h \theta} = 0.15$$

is distributed uniformly between the four nodes at the junction between the neural plate and the epithelium. No other forces (including apical microfilament forces) are applied, although axial elongation is still imposed. The physical basis for the production of such a medial force is not clear, but it seems significant that the final simulated shape bears a strong resemblance to the transverse section through a chick embryo treated with cytochalasin D to arrest microfilament contraction, as shown by Schoenwolf and Smith (1990, Fig. 18).

Simulations of surgical interventions

A variety of surgical interventions were simulated to further investigate the notion that CMBs provide the primary driving force. These include simulations of an excised plate, an excised plate prevented from rolling, and an in vivo neural plate from which one of the prospective ridges has been extirpated.

Excised plate

One of the classical ways to determine the intrinsic behaviour of the neural plate is to excise it (Roux 1888; Jacobson and Gordon 1976; Lee and Nagele 1988). A simulation of an excised plate is shown in Fig. 7. The geometry, driving forces, and rate of axial elongation acting on this plate exactly match those of the neural plate portion of the reference case. This simulation shows that an excised plate with apical microfilaments would exhibit a uniform curvature across its surface at any instant in time, and would roll up quickly. Minimal thickening is visible, no cell skewing occurs, no ridges nor hinges develop, and closure takes place before significant axial elongation occurs. These features are consistent with comparable experimental data (Jacobson and Gordon 1976; Schoenwolf and Smith 1990).

If microfilaments formed along the base of the explant, they would counteract apical constriction and slow or prevent rolling. If sufficient microfilaments formed on the newly-exposed basal surface, the explant would roll the opposite way.

Excised plate prevented from rolling

What happens if an excised neural plate is prevented from rolling? Burt (1943) reports that cell elongation still occurs. The simulation shown in Fig. 8 is identical to the excised plate simulation, except that rolling is prevented by constraining the base of all cells so that they can move only horizontally. As shown, the neural tissue still thickens and narrows. Some cell

Fig. 7. Excised plate. This simulation shows that, under the action of apical microfilaments, an excised plate (A) rolls up (B and C) in such a way that at any instant the curvature is uniform over the surface of the plate.

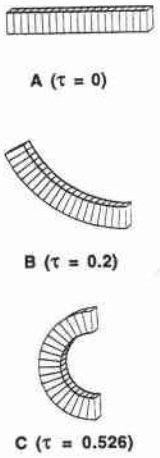

Fig. 8. Excised plate prevented from rolling. When an excised plate and attached epithelium (A) are prevented from rolling, the neural plate thickens and the cells at the lateral edge of the plate skew (B).

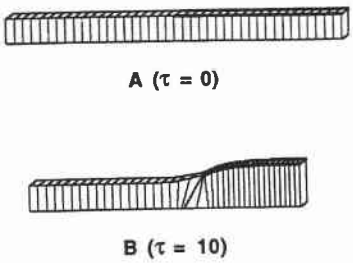

skewing is apparent at the junction between the neural and nonneural tissues.

Slitting experiment

Numerous experiments have been performed in which parts of the neural plate are extirpated or slits are made near or in it (Lewis 1947; Jacobson 1962; Karfunkel 1974). As an example of this type of experiment, we consider the experiment of Jacobson and Gordon (1976), in which they removed the prospective neural ridge and some adjacent neural plate cells from one side of a stage 13 *Taricha torosa* embryo. They then fixed and sectioned the embryo at stage 15.

A simulation of a slit plate or of a plate that has had its medial edge extirpated is shown in Fig. 9. The geometry of the left side of the plate is identical to that of the reference case, except that the center of the plate is fixed only along its basal surface. In addition, 10 volume elements with corresponding apical microfilament elements have been added to model the incomplete right side of the neural plate. The bases of the four elements that are anchored at the notochord at the embryo centerline are shown with wider lines. The simulation show that cells overlying the notochord skew by approximately the same amount (23°) as the corresponding cells measured by Jacobson and Gordon (1976).

Fig. 9. A slitting experiment. Here, the left side of a neural plate with its attached nonneural epithelium and part of the right side of the neural plate are modelled (A). The widened lines on the basal surface indicate the position of the notochord where the neural plate cells are assumed to be anchored. This simulation demonstrates that if a slit parallel to the cephalo–caudal axis were made towards the right lateral side of the neural plate, or if the right presumptive neural ridge were extirpated, apical microfilaments would produce significant shape changes as shown (B). Cell skewing is visible above the notochord and at the right edge (B).

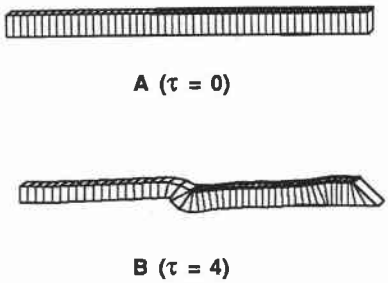

Discussion

The simulations reported here demonstrate that complex sequences of shape changes can be produced by mechanical means alone. For example, the sequence of shape changes shown in Fig. 2 results entirely from coupling between the force generators (apical microfilaments) and the changing shape of the cell sheet (Clausi and Brodland 1993). As the neural plate and attached ectoderm change shape, the force generators have a continually changing effect on them. Thus, when the cell sheet is flat, microfilaments cause an ogee shape to form at the edge of the neural plate. When the ogee is fully developed, the same driving forces cause plate narrowing. Finally, when sufficient plate narrowing and thickening has occurred, these force generators cause the plate to roll up into a tube.

The simulations also demonstrate that when different driving forces or boundary conditions act on otherwise identical tissues, distinct patterns of shape change result (Figs. 2, 3, 4, 6, and 8). The substantial differences between Figs. 2 and 4 demonstrate that the simulation results are even sensitive to such apparently minor details as whether or not microfilament bundle contraction forces change as the bundle shortens. In addition, the sequences of shapes produced by simulations of neurulation (Fig. 2), teratogen treatments (Fig. 6), and surgical manipulations (Figs. 7–9) agree well with corresponding experimental results. These factors suggest that the simulations can be used with some confidence to investigate the cytoskeletal mechanics of neurulation.

Surgical experiments have played an important role in elucidating the mechanics of neurulation. However, in such experiments, the possibility exists that factors other than those that are the subject of the experiment might affect the results. Computer simulations are useful in such cases because they allow specific changes to be made without concern that other factors are also being altered.

For example, microfilaments are known to develop quickly in cells that cover newly exposed tissue surfaces. Thus, when explants are made or slits are cut it is likely that any resulting motions are affected by microfilaments that form in cells on

the newly exposed surfaces. Simulations were carried out of excised neural plates (Figs. 7 and 8) and of a slitting experiment (Fig. 9). In these simulations, newly exposed surfaces were not assumed to be covered with microfilaments. That the simulations agree well with corresponding experiments suggests that the influence of any newly formed microfilaments or other factors are negligible in these particular experiments.

The simulations of neurulation and surgical experiments reported here support the hypothesis that apical microfilaments are a primary force generator. However, even though the right detailed sequence of shape changes are produced by the joint action of CMBs and axial elongation, this does not prove that these are the normal or sole driving forces. Other patterns of force generation could possibly be contrived that would produce sequences of shape change which are not discernibly different. However, it is highly unlikely that such alternate patterns of force generation occur in vivo.

The simulations also support the argument that multiple sets of force generators act during neurulation. For example, a variety of experimental observations suggest that neurulation motions might be assisted by medial motions of adjacent tissues (Jacobson 1962; Jacobson and Löfberg 1969; Jacobson and Jacobson 1973). In addition, Schoenwolf et al. (1988) state that in the absence of apical microfilaments, neurulation-like movements can still occur. The simulation shown in Fig. 6 shows the shape changes that would occur if apical microfilaments were absent and a medial force were applied at the edge of the neural plate. That the shapes produced in the simulation agree with the experiment of Schoenwolf and Smith (1990), in which microfilaments were depolymerized using cytochalasin D, supports the concept that forces may be produced by or transmitted through the adjacent tissues.

Embryonic cells are in mechanical contact with each other and can be thought of as sending mechanical signals to each other through force interactions. The characteristic sequences of shapes produced in the simulations are dependent on these mechanical interactions. As the various parts of an embryo change shape during development, local geometries and mechanical behaviours are altered. This, in turn, affects their future mechanical behaviour and thus, the developmental pathways available. For example, the simulations shown in Figs. 2 and 3 demonstrate that differences in reshaping give rise to differences in neural-plate thickening and that this ultimately affects the local rate of tube closure. Similar phenomena are also observed in nonbiological, plate- and shell-like structures (Brodland 1988; Brodland and Cohen 1989). The patterns of mechanical development available at any instant of embryo development are dependent on the previous mechanical history of the embryo. Thus, a mechanical basis for an epigenetic landscape exists. Critical biochemical changes may be initiated by these mechanical events (Ben Ze'ev 1985) and may further alter the characteristics of this landscape.

Computer simulations provide a complement to experimental studies of neurulation. In particular, they allow the mechanical merits of specific theories to be evaluated. One of the features of computer simulations is that they allow the construction and testing of mechanical systems that may not be possible to test in vivo. Thus, computer simulations allow the mechanics of any theory of neurulation, including ones for which no physical evidence has yet been found, to be examined.

The efficacy of suitably formulated finite element methods for modelling mechanical aspects of morphogenesis has been demonstrated. A possible next step would be to use finite element-based simulations to investigate morphogenetic phenomena in which biochemical or other nonmechanical cell–cell communication are known to be crucial. The finite element method is sufficiently general as a modelling tool that such factors might be incorporated. Interactions between mechanical and nonmechanical phenomena may then be investigated.

Acknowledgment

This research was funded by the Natural Sciences and Engineering Research Council of Canada.

References

Alberts, B., Bray, D., Lewis, J., Raff, M., Roberts, K., and Watson, J. 1989. Molecular biology of the cell. 2nd ed. Garland Publishing, Inc., New York.

Balinsky, B.I. 1961. Ultrastructural mechanisms of gastrulation and neurulation. Symposium on germ cells and development. A. Baselli, Milan. p. 550.

Belytschko, T., and Ong, J.S. 1984. Hourglass in linear and nonlinear problems. Comp. Methods Appl. Mech. Eng. **43**: 251–276.

Ben-Ze'ev, A. 1985. Cell–cell interaction and cell configuration-related control of cytokeratins and vimentin expression in epithelial cells and in fibroblasts. Ann. N.Y. Acad. Sci. **455**: 597–613.

Brodland, G.W. 1988. Highly non-linear deformation of uniformly-loaded circular plates. Int. J. Solids. Struct. **24** (No. 2): 351–362.

Brodland, G.W. 1994. Finite element methods for developmental biology. *In* The cytoskeleton in development biology. Int. Rev. Cytol. **150**: 95–118.

Brodland, G.W., and Clausi, D.A. 1994. Embryonic cell sheet morphogenesis modelled by FEM. ASME J. Biomech. Eng. **116**: 146–155.

Brodland, G.W., and Cohen, H. 1989. Deflection and snapping of ring-loaded spherical caps. ASME J. Appl. Mech. **111** (No. 56) 127–132.

Brodland, G.W., and Gordon, R. 1990. Intermediate filaments may prevent buckling of compressively-loaded microtubules. J. Biomech Eng. **112**: 319–321.

Brodland, G.W., and Shu, D.-W. 1992. Are intercellular membrane forces important to amphibian neurulation? *In* Dynamical phenomena at interfaces, surfaces and membranes. *Edited by* G. Forgacs and D. Beysens. Nova Science Publishers, New York.

Brun, R.B., and Garson, J.A. 1983. Neurulation in the Mexican salamander (*Ambystoma mexicanum*): a drug study and cell shape analysis of the epidermis and the neural plate. J. Embryol. Exp. Morphol. **74**: 275–295.

Burnside, B. 1971. Microtubules and microfilaments in newt neurulation. Dev. Biol. **26**: 416–441.

Burnside, B. 1973. Microtubules and microfilaments in amphibian neurulation. Amer. Zool. **13**: 989–1006.

Burnside, M.B., and Jacobson, A.G. 1968. Analysis of morphogenetic movements in the neural plate of the newt Taricha torosa. Dev. Biol. **18**: 537–552.

Burt, A. 1943. Neurulation in mechanically and chemically inhibited amblystoma. Biol. Bull. (Woods Hole, Mass.), **85**: 108.

Campbell, L.R., Dayton, D.H., and Sohal, G.S. 1986. Neural tube defects: a review of human and animal studies on the etiology of neural tube defects. Teratology **34**: 171–187.

Clausi, D.A., and Brodland, G.W. 1993. Mechanical evaluation of theories of neurulation using computer simulations. Development **118**: 1013–1023.

Copp A.J., Brook F.A., Estibeiro P., Shum A.S.W., and Cockroft D.L. 1990. The embryonic development of mammalian neural tube defects. Prog. in Neurobiol. **35**: 363–403.

Gordon, R. 1985. A review of the theories of vertebrate neurulation and their relationship to the mechanics of neural tube birth defects. J. Embryol. Exp. Morphol. **89**: (Suppl.) 229–255.

Hart, T.N., and Trainor, L.E.H. 1990. The two-component model for the cytoskeleton in development, Physica D (Amsterdam), **44**: 269–284.

Hilfer, S.R., and Hilfer, E.S. 1983. Computer simulation of organogenesis: an approach to the analysis of shape changes in epithelial organs. Dev. Biol. **97**: 444–453.

Hill, T.L. 1981. Microfilament or microtubule assembly or disassembly against a force. Proc. Natl. Acad. Sci. U.S.A. **78**: 5613–5617.

Hill, T.L., and Kirschner, M.W. 1982*a*. Subunit treadmilling of microtubules or actin in the presence of cellular barriers: possible conversion of chemical free energy into mechanical work. Proc. Natl. Acad. Sci. *U.S.A.* **79**: 490–494.

Hill, T.L., and Kirschner, M.W. 1982*b*. Bioenergetics and kinetics of microtubules and actin filament assembly-disassembly. Int. Rev. Cytol. **78**: 1–125.

Hiramoto, Y. 1969. Mechanical properties of the protoplasm of the sea urchin egg. I. Unfertilized egg. Exp. Cell Res. **56**: 201–208.

His, W. (1874). Unsere Körperform und das physiologische problem ihrer enstehung, briefe an einen befreundeten naturforscher. F.C.W. Vogel, Leipzig.

Huebner, K.H., and Thornton, E.A. 1982. The finite element method for engineers. 2nd ed. John Wiley and Sons, Toronto.

Jacobson, A.G. 1978. Some forces that shape the nervous system. Zoon, **6**: 13–21.

Jacobson, A.G. 1980. Computer modelling of morphogenesis. Am. Zool. **20**: 669–677.

Jacobson, A.G., and Gordon, R. 1976. Changes in the shape of the developing vertebrate nervous system analyzed experimentally, mathematically and by computer simulation. J. Exp. Zool. **197**: 191–246.

Jacobson, A.G., Oster, G.F., Odell, G.M., and Cheng, L.Y. 1986. Neurulation and the cortical tractoring model for epithelial folding. J. Embryol. Exp. Morphol. **96**: 19–49.

Jacobson, C.O. 1962. Cell migration in the neural plate and the process of neurulation in the axolotl larva. Zool. Bidr. Uppsala, **30**: 433–449.

Jacobson, C.O., and Jacobson, A. 1973. Studies on morphogenic movements during neural tube closure in amphibia. Zoon, **1**: 17–21.

Jacobson, C.O., and Löfberg, J. 1969. Mesoderm movements in the amphibian neurula. Zool. Bidrag (Uppsala) **38**: 233–239.

Karfunkel, P. 1974. The mechanisms of neural tube formation. Int. Rev. Cytol. **38**: 245–271.

Koehl, M.A.R. 1990. Biomechanical approaches to morphogenesis. Semin. Dev. Bio. **1**: 367–378.

Lee, H., and Nagele, R.G. 1988. Intrinsic forces alone are sufficient to cause closure of the neural tube in the chick. Experientia (Basel), **44**: 60–61.

Lewis, W.H. 1947. Mechanics of invagination. Anat. Rec. **97**: 139–156.

Liu, W.K., Ong, J.S., and Uras, R.A. 1985. Finite element stabilization matrices — a unification approach. Comp. Methods Appl. Mech. Eng. **53**: 13–46.

Logan, D.L. 1986. A first course in the finite element method, 1st ed. Prindle, Weber, Schmidt (PWS) Publishers, Boston, Mass.

Odell, G.M., Oster, G., Alberch, P., and Burnside, B. 1981. The mechanical basis of morphogenesis. I. Epithelial folding and invagination. Dev. Biol. **85**: 446–462.

Rappaport, R. 1977. Tensiometric studies of cytokinesis in cleaving sand dollar eggs. J Exp. Zool. **201**: 375–378.

Roux, W. 1888. Beiträge zur entwickelungsmechanik des embryo. Über die künstliche hervorbringung halber embryonen durch zerstörung einer der beiden ersten furchungskugeln, sowie über die nachentwickelung (postgeneration) der fehlenden köperhälfte. Virchows Arch. Path. Anat. Physiol. Klin. Med. **114**: 113–153, 289–291.

Schoenwolf, G.C., and Smith, J.L. 1990. Mechanisms of neurulation: traditional viewpoint and recent advances. Development (Cambridge), **109**: 243–270.

Schoenwolf, G.C., Folsom, D., and Moe, A. 1988. A reexamination of the role of microfilaments in neurulation in the chick embryo. Anat. Rec. **220**: 87–102.

Smith, J.L., and Schoenwolf, G.C. 1991. Further evidence of extrinsic forces in bending of the neural plate. J. Comp. Neurol. **307**: 225–236.

Valerg, P.A., and Alvertini, D.F. 1985. Cytoplasmic motions, rheology, structure probed by a novel magnetic particle method. J. Cell. Biol. **101**: 130–140.

Weliky, M., and Oster, G. 1990. The mechanical basis of cell rearrangement I. Epithelial morphogenesis during Fundulus epiboly. Development (Cambridge), **109**: 373–386.

Zienkiewicz, O.C., and Taylor, R.L. 1989. The finite element method, basic formulation and linear problems. Vol. 1. 4th ed. McGraw-Hill, London.

Zienkiewicz, O.C., and Taylor, R.L. 1991. The finite element method, solid and fluid mechanics dynamics and non-linearity. Vol. 2. 4th ed. McGraw-Hill, London.